Phase asymmetry guided adaptive fractional-order total variation and diffusion for feature-preserving ultrasound despeckling

Kunqiang Mei, Bin Hu, Baowei Fei, and Binjie Qin*, *Member, IEEE*

***Abstract*—It is essential for ultrasound despeckling to remove speckle noise while simultaneously preserving edge features for accurate diagnosis and analysis in many applications. To preserve real edges such as ramp edges and low contrast edges, we first detect edges using a phase-based measure called phase asymmetry (PAS), which can distinguish small differences in transition border regions and varies from 0 to 1, taking 0 in ideal smooth regions and taking 1 at ideal step edges. We further propose three strategies to properly preserve edges. First, in observing that fractional-order anisotropic diffusion (FAD) filter has good performance in smooth regions while the fractional-order TV (FTV) filter performs better at edges, we leverage the PAS metric to keep a balance between FAD filter and FTV filter for achieving the best performance of preserving ramp edges. Second, considering that the FAD filter fails to protect low contrast edges by solely integrating gradient information into the diffusion coefficient, we integrate the PAS metric into the diffusion coefficient to properly preserve low contrast edges. Finally, different from fixed fractional order diffusion filters neglecting the differences between smooth regions and transition border regions, an adaptive fractional order is implemented based on the PAS metric to enhance edges. The experimental results show that our method outperforms other state-of-the-art ultrasound despeckling filters in both speckle reduction and feature preservation.**

***Index Terms*—Ultrasound images, speckle noise, FAD filter, FTV filter, phase asymmetry, fractional order.**

I. Introduction

ULTRASOUND imaging is a widely used medical-imaging modality due to its noninvasive, low cost and convenient. However, the quality of ultrasound images is relatively low compared with other medical imaging modalities. The main reason of quality degradation in ultrasound images is the presence of an inherent imaging artifact called speckle, which results from constructive and destructive coherent interferences of backscattered echoes from the scatterers [1]. Speckle is commonly interpreted as a locally correlated noise that reduces image contrast and conceals fine feature details [2], causing negative effects on medical diagnosis and reducing the accuracy of subsequent image processing such as segmentation and registration. Furthermore, extracting coherent feature patterns from the noisy ultrasound signals is necessary for super-resolution ultrasound microvessel imaging [3] and 3D reconstruction from a series of 2D freehand ultrasound image [4]. Therefore, it is very important to remove speckle noise with satisfactory feature preservation for accurate diagnosis and analysis in many applications.

However, feature-preserving speckle reduction is a challenge task, since speckle noise is known to be tissue-dependent and it manifests itself in the form of multiplicative noise [5], [6], [7], which means that the intensity of speckle can change sharply. Therefore, just employing intensity-based gradient information cannot accurately distinguish edges from speckle noise, especially for the edges with low contrast. Failing to preserve edge features will damage other features that are made of by the edges. Existing edge-preserving image processing techniques [8], [9] are likely to damage some low contrast features, since they regard some low contrast edges as speckle noise and remove these edges after noise removal by exploring intensity-based gradient information.

Various speckle reduction filters are proposed to solve the above-mentioned challenges, including local adaptive filters, non-local means (NLM) filters and diffusion filters. The local adaptive filters such as Frost [9] filters rectify a pixel by averaging its neighboring pixels. Later, the squeeze box filter (SBF) [10] rectify only local extrema at each iteration by replacing them with the local mean. However, local adaptive filter is sensitive to the shape and size of local windows. The non-local means (NLM) algorithms assume that natural images contain many similar features. NLM algorithms group similar features from different image patches and remove noise by a weighted average of similar features. Coupe et al. [11] proposed the optimal Bayesian NLM (OBNLM) filter to process ultrasound images. Recently, Zhu et al. [12] developed a non-local low-rank framework (NLLRF) for ultrasound speckle reduction, which leverages a guidance image to improve the performance of patch selection. However, NLM algorithms usually mix different features into the same cluster in the case of large number of features, causing some important details becoming indiscernible after noise removal [13].

As for diffusion filtering, after Perona and Malik proposed the well-known anisotropic diffusion (AD) filter [14], both speckle reducing anisotropic diffusion (SRAD) [15] filter and detail preserving anisotropic diffusion (DPAD) [16] filter are modified based on the AD filter. SRAD filter added a parameter related to the noise estimate into the diffusion coefficient,

Kunqiang Mei and Binjie Qin are with the School of Biomedical Engineering, Shanghai Jiao Tong University, Shanghai, 200240, China. e-mail: bjqin@sjtu.edu.cn.

Bin Hu is with Department of Ultrasound in Medicine, Shanghai Jiao Tong University Affiliated Sixth Peoples Hospital, Shanghai Institute of Ultrasound in Medicine, Shanghai, 200233, China.

Baowei Fei is with Erik Jonsson School of Engineering and Computer Science, University of Texas at Dallas, Richardson, TX 75080, USA.

Manuscript received April 19, 2018; revised August 26, 2018.

while DPAD filter adopted an improved noise estimator to improve the despeckling performance of SRAD filter. The oriented speckle reducing anisotropic diffusion (OSRAD) [17] filter modified the diffusion coefficient with the local directional variance of image intensity. However, all these diffusion filters employ intensity-based gradient information to identify edges, failing to preserve low contrast edges. Moreover, these filters tend to produce staircase effect. To reduce the staircase effect, Bai and Feng [18] proposed a fixed fractional-order AD (FAD) model for image denoising. Nevertheless, the fixed fractional-order diffusion filter neglects the differences among various image regions. Recently, Flores et al. [2] developed an anisotropic diffusion filter guided by the log-Gabor filters (ADLG) instead of intensity-based gradient. However, ADLG fails to achieve satisfactory feature preservation.

In summary, above-mentioned diffusion filters failing to accurately identify edges cannot achieve satisfactory feature preservation. Being an important image feature, edge is a basic element of other features, such as ridges and textures, such that failing to preserve the edges will render these features inviable [19], [20]. To solve the drawback of intensity-based edge detector, some local phase-based edge detection methods [21][22] were developed in ultrasound images. Local phase information can be obtained by convolving the image data with a pair of band-pass quadrature filters. We then can construct a local phase-based feature indicator called phase symmetry (PS) or phase asymmetry (PAS) depending on the image feature type to be detected [23]. Specifically, PS can be used to detect symmetry features for image enhancement, such as bone surface enhancement [24] and vessel enhancement [25] while PAS can be used to identify edge features for ultrasound image denoising [21] and segmentation [22]. Inspired by these works [21][22], we also use the phase asymmetry to detect edge information. In ultrasound images, almost all of real edges are ramp edges of various slopes rather than ideal step edges. Especially, low contrast edges refer to the ramp edges with low step amplitude.

Both PS and PAS are special patterns of phase congruency (PC) [26] and developed on the postulation that features are perceived at points where their Fourier components are maximal in phase. Using Fourier analysis, we can detect a wide range of feature type, such as step edges and lines. We just employ PAS measure to detect edges in the image. As for symmetry features, they are also made of edges. If we protect their edges, symmetry features will be preserved properly.

It has been shown that PAS measure can effectively separate edges from smooth regions in many applications [21][22]. The PAS metric represents the edge significance of each point and varies from 0 to 1, taking 0 (indicating no significance) in ideal smooth regions and taking 1 (indicating a very significant edge point) at ideal step edges. In general, points at the same edge have the similar edge significance. As the steepness of a ramp edge reduces, the PAS values of the edge points also reduce. Thus, we can also distinguish different ramp edges based on the PAS values of edge points. This work makes a threefold contribution closely associated with the PAS metric:

1. To take full advantage of FAD and FTV filters, we utilize PAS metrics as weighting coefficients to get a performance balance between FAD filter and FTV filter in achieving the best ultrasound despeckling and ramp edge preservation. This PAS-based weighted coefficients not only accurately discern edges and smooth regions but also precisely differentiate varieties of ramp edges.
2. We integrate the PAS metric into the diffusion coefficient of FAD filter to preserve low contrast edges. Traditional diffusion filters solely employ intensity-based gradient information to identify edges, failing to preserve low contrast edges after noise removal. To solve this problem, we add the PAS metric to the diffusion coefficient to properly preserve low contrast edges.
3. Our framework adjusts the fractional order adaptively based on the PAS metrics to enhance various edges. Diffusion filters tend to reduce the edge contrast during the smoothing process. Although fixed fractional order diffusion filters can enhance various edges, they neglect the differences between smooth regions and transition border regions. If we apply high order fractional differentials on the whole image without discerning edges and smooth regions, edges will be enhanced but at the same time smooth regions will be ignored [27], [28]. Our adaptive strategy adopts high fractional order for edges and uses low fractional order for smooth regions. Furthermore, considering different edge points have different significance, our framework assigns different fractional order to each edge point for obtaining a better edge enhancement.

By designing the weighted coefficients, the diffusion coefficient and the adaptive fractional order based on the PAS metrics, our method not only achieves more excellent quantitative despeckling performance but also performs better in preserving features via visual evaluation when compared with other state-of-the-art speckle reduction filters. In this paper, phase asymmetry, fractional order differential and fractional-order AD and TV filters are introduced in Section II. The details of our method are introduced in Section III. The experimental results are reported in Section IV. We further discuss some issues and summarize this work in Section V.

II. THEORETICAL BACKGROUND

A. Phase Asymmetry

For the characteristics of ultrasound images, solely employing gradient information to identify edges cannot achieve satisfactory feature preservation. This work detects edges by adopting phase-based PAS measure, which can efficiently separate edges from smooth regions. According to a human perception study [23], at the points of perceivable step edges, the absolute values of even symmetric filter responses are small while the absolute values of odd symmetric filter responses are large. In other words, the difference between the odd and the even filter responses is large. According to this finding, PAS [23] was developed to detect step edges.

To calculate the PAS metric of a 2D signal f, we first need to extract its local phase and local amplitude. The monogenic signal [29] was proposed to decompose the 2D signal f into local phase and local amplitude based on

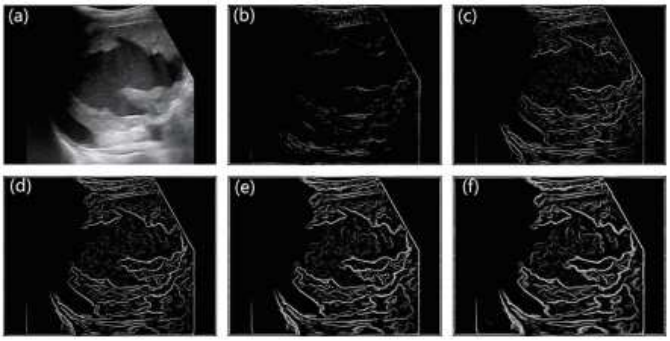

Fig. 1. Example of PAS measure at different scales. (a) The ultrasound image of the spleen; the PAS map of: (b) $s = 5$, (c) $s = 10$, (d) $s = 15$, (e) $s = 20$, (f) $s = 25$.

Riesz filters. The monogenic signal f_M is defined as: $f_M = (f, f_R) = (f, r_1 * f, r_2 * f)$, where f_R is the Riesz transform of f, $r_1(x_1, x_2)$ and $r_2(x_1, x_2)$ are the spatial representation of Riesz filters shown as

$$\begin{aligned} r_1(x_1, x_2) &= \frac{-x_1}{2\pi\left(x_1^2+x_2^2\right)^{3/2}} \\ r_2(x_1, x_2) &= \frac{-x_2}{2\pi\left(x_1^2+x_2^2\right)^{3/2}} \end{aligned} \tag{1}$$

Since natural images generally contain a wide range frequencies, the monogenic signal f_M needs to combine with a set of bandpass quadrature filters b. The monogenic signal f_M becomes $f_M = (b * f, b * r_1 * f, b * r_2 * f) = (even, odd)$, where $even$ and odd denote the scalar-valued even and vector-valued odd filter responses.

Several families of bandpass filters b have been proposed to calculate the $even$ and odd, we adopt a Cauchy kernel as the bandpass filter, since Cauchy kernel has analytical expression in the spatial and the Fourier domain [30]. In the frequency domain, the 2D isotropic Cauchy kernel is defined by

$$C(w) = n_c \left|w\right|^a \exp\left(-s\left|w\right|\right), a \geq 1 \tag{2}$$

where $w = (w_1, w_2)$ is the angular frequency, s is the scaling parameter, $n_c = \left(\frac{\pi\, 4^{a+1}\, s^{2a+1}}{\Gamma(2a+1)}\right)^{\frac{1}{2}}$, $\Gamma(\cdot)$ is the gamma function, and a is the bandwidth. We set $a = 1.58$, as suggested in [21].

To detect step edges accurately, Kovesi [23] suggested to use the PAS measure over a number of scales. Therefore, we define the multiple scales PAS as follows:

$$PA = \sum_s \frac{\lfloor |odd_s| - |even_s| - T_s \rfloor}{\sqrt{even_s^2 + odd_s^2} + \varepsilon} \tag{3}$$

where T_s is the scale specific noise threshold [21], ε is a small positive number, $\lfloor \cdot \rfloor$ represents zeroing of negative values, PA is the PAS metric, and s is the scaling parameter of Cauchy kernels. Specifically, s plays an important role in obtaining an accurate edge map, since increasing s will regularize the continuity (or connect the breakpoints) in the boundaries but lose details somewhat in edge detection. Fig. 1 shows an example of PAS measure at different scales. We can find that the discontinuities in some boundaries in the PAS maps at $s = 5$ and $s = 10$ will reduce the accuracy of locating edges. The boundaries in the PAS maps at $s = 20$ and $s = 25$ have good continuity but some details are lost. The PAS map at $s = 15$ maintains a balance between the boundary continuity and detail preservation. Thus, we choose $s = 15$ to detect edges in real ultrasound images.

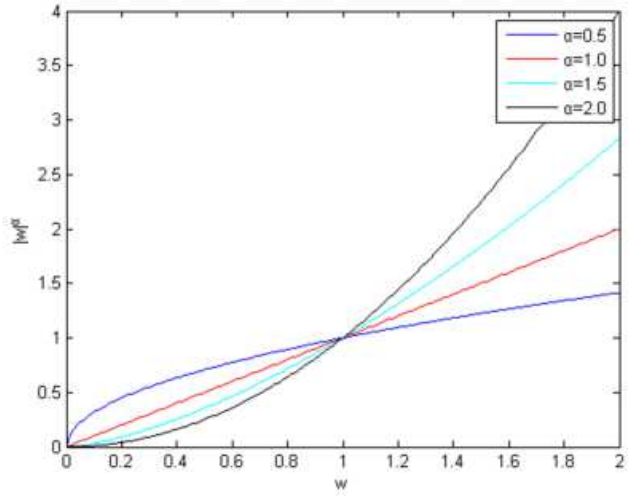

Fig. 2. The curves of the amplitude-frequency characteristic of fractional differential with different orders.

PAS provides an absolute measure of the edge significance of points. The PAS metric varies from 0 to 1, taking 0 (indicating no significance) in ideal smooth regions and taking 1 (indicating a very significant edge point) at ideal step edges. In general, points at the same edge have the similar edge significance. As the steepness of a step edge reduces, the PAS values of the edge points also reduce. Due to PAS being invariant to brightness or contrast, low contrast edges can be detected efficiently. For the real ramp edges in ultrasound images, the PAS values of these edge points are less than 1.

B. Fractional order differential

Compared with integer order differential, fractional order differential performs better in enhancing edges during image processing [28]. For a square differentiable signal $f(x) \in L^2(R)$, its fractional order differential is given as

$$D^\alpha f(x) = \frac{d^\alpha f(x)}{d\, x^\alpha} \tag{4}$$

where α is a positive real number. The Fourier transform of $D^\alpha f(x)$ is

$$\begin{aligned} D^\alpha f(x) \overset{FT}{\Leftrightarrow} (\hat{D}^\alpha f)(w) &= (iw)^\alpha \hat{f}(w) \\ &= |w|^\alpha \exp\left[i\,\theta^\alpha(w)\right] \hat{f}(w) \\ &= |w|^\alpha \exp\left[\frac{\alpha\pi i}{2}\mathrm{sgn}(w)\right] \hat{f}(w) \end{aligned} \tag{5}$$

where w is the angular frequency, $\mathrm{sgn}(\cdot)$ denotes the numeric symbol of the integer part, and $(iw)^\alpha = |w|^\alpha \exp\left[\frac{\alpha\pi i}{2}\mathrm{sgn}(w)\right]$ is the filter function of fractional differential filter. According to the filter function, we can draw the curves of the amplitude-frequency characteristic of fractional differential with different α as depicted in Fig. 2. From Fig. 2, it is obviously seen that in the low frequency field

with $0 < w < 1$, the fractional differential acts as an attenuation function. Nevertheless, in the section with $w > 1$, the fractional differential enlarges the amplitude values, and the enhanced amplitude will be stronger as the fractional order α increases. Taking into account the amplitude enhancement in the high frequency field, we effectively apply the fractional order differential into edge enhancement in image denoising.

Diffusion filters tend to reduce the edge contrast during smoothing. Although traditional fractional-order diffusion filters usually adopt one fixed fractional order to process the image, this strategy neglects the differences between smooth regions and transition border regions [28]. Edges will be weakened if a low fractional order is used, while smooth regions will be ignored if a high fractional order is adopted. This drawback will inevitably cause some details to be damaged after noise removal [27]. Therefore, a more reasonable choice is to assign the fractional order α adaptively based on the local image information.

Currently, there are three commonly used definitions of fractional calculus: the Capotu definition, the GrünwaldLetnikov (G-L) definition and the RiemannLiouville (R-L) [31], [32]. Since the G-L definition expresses a function using weighted sum around the function, the G-L definition is suitable for applications in signal processing. According to [33], α-order differential of signal $f(x)$ was defined by the G-L as:

$$D^{\alpha}f(x) \triangleq \lim_{h\to 0}\frac{1}{h^{\alpha}}\sum_{k=0}^{[\frac{d-c}{h}]}(-1)^{l}\binom{\alpha}{l}f(x-lh) \tag{6}$$

where α is the fractional order, $[c,d]$ is the duration of $f(x)$, the integer part of $\frac{d-c}{h}$ is $[\frac{d-c}{h}]$, and the formula $\binom{\alpha}{l}$ is the binomial coefficient defined as

$$\binom{\alpha}{l} = \frac{\Gamma(\alpha+1)}{\Gamma(l+1)\Gamma(\alpha-l+1)} \tag{7}$$

where $\Gamma(n) = (n-1)!$ is the gamma function.

C. Fractional-order AD filter and fractional-order TV filter

The following partial differential equation defines the AD [14] filter

$$\frac{\partial u}{\partial t} = div\left[c\left(|\nabla u|\right)\cdot\nabla u\right], \tag{8}$$

where div is the divergence operator, $|\nabla u|$ is the absolute value of ∇u, and $c(\cdot)$ is the diffusion coefficient related the magnitude of local image gradient ∇u. A possible diffusion coefficient function [14] is defined as

$$c\left(|\nabla u|\right) = 1/\left[1+|\nabla u|^{2}/k^{2}\right] \tag{9}$$

where k is the gradient threshold. To preserve edges, this diffusion coefficient will reduce the diffusivity at edges which have large magnitude of local intensity-based gradient.

The TV filter [34] is proposed as

$$E(u) = \int_{\Omega}\left(|\nabla u| + \frac{\lambda}{2}|u-u_0|^{2}\right) \tag{10}$$

where $|\nabla u|$ denotes the total variation, $|u-u_0|^2$ is the fidelity term, λ is the regularization parameter and u_0 is the noisy image.

To reduce the staircase effect that is alway caused by AD and TV filters, FAD [18] filter and FTV [35] filter were developed. The FAD filter[18] is shown as

$$E\left(\mathrm{u}\right) = \int_{\Omega} f\left(|\nabla^{\alpha}u|\right)d\Omega \tag{11}$$

where α is the fractional order, $\nabla^{\alpha}u = \left(\nabla_x^{\alpha}u, \nabla_y^{\alpha}u\right)$, $|\nabla^{\alpha}u| = \sqrt{\left(\nabla_x^{\alpha}u\right)^2 + \left(\nabla_y^{\alpha}u\right)^2}$, and $f\left(|\nabla^{\alpha}u|\right) \geq 0$ is an increasing function associated with the diffusion coefficient in the AD [14] filter shown as

$$c\left(t\right) = \frac{f'\left(\sqrt{t}\right)}{\sqrt{t}} \tag{12}$$

Zhang and Wei [35] proposed the following FTV filter

$$E\left(u\right) = \int_{\Omega}\left(|\nabla^{\alpha}u| + \frac{\lambda}{2}|u-u_0|^{2}\right)dxdy \tag{13}$$

where α is the fractional order, $|\nabla^{\alpha}u|$ denotes the total variation, $|u-u_0|^2$ is the fidelity term, λ is the regularization parameter and u_0 is the noisy image.

III. Proposed APPROACH

A. The proposed model

This paper proposes a phase asymmetry guided adaptive fractional-order total variation and diffusion filter for feature-preserving ultrasound despeckling. The proposed filter combines equation (11) and (13) to balance FAD filter and FTV filter for achieving the best performance of preserving ramp edges, and the energy function is defined as follows

$$E\left(u\right) = \int_{\Omega}\left[\varphi f\left(|\nabla^{\alpha}u|\right) + \gamma|\nabla^{\alpha}u| + \frac{\lambda}{2}|u-u_0|^{2}\right]dxdy \tag{14}$$

where α is the adaptive fractional order, φ and γ are the weighted coefficients, which control the relative importance of FAD filter and FTV filter, and λ is the regularization parameter. We empirically set λ as 0.01. As for the weighted coefficients, we design them based on the PAS metric shown as

$$\begin{cases} \varphi = (PA-1)^2 \\ \gamma = PA(2-PA) \end{cases} \tag{15}$$

where PA is the PAS metric that is updated in each iteration for accurately obtaining the edge significance of each point.

Based on the above strategy, when PA is close to 0, we emphasize the role of FAD filter in smooth regions. When PA is close to 1, we highlight the role of FTV filter in the transition border regions. Due to the PA values of edge points for real ramp edges being less than 1, the FAD filter also plays a key role in processing these transition border regions.

However, FAD filter solely integrates intensity-based gradient information into the diffusion coefficient, causing some low contrast edges being removed after noise removal. To overcome this drawback, we integrates the PAS metric into the diffusion coefficient. PAS measure can efficiently identify low

contrast edges due to its invariant to brightness or contrast. Furthermore, the value of PAS metric is only related to the edge significance of each point. We alter the function $f\left(|\nabla^{\alpha} u|\right)$ by modifying its diffusion coefficient $c(\cdot)$ according to (12). The modified diffusion coefficient is shown as:

$$c(|\nabla^{\alpha} u|, PA) = 1/[1 + \frac{|\nabla^{\alpha} u| \cdot (1 + 254 \cdot PA)}{k_1^2}] \quad (16)$$

where $k_1 = k_0\, e^{-0.05(n_{iter}-1)}$ is the modified version of k in (9). Here n_{iter} is the number of iterations, k_0 is a positive constant that is related to the noise level.

Owing to diffusion filters reducing the edge contrast during smoothing, it is essential to design proper strategy to enhance various edges in ultrasound image. According to the discussion in Sec.II-B, we can assign the fractional order adaptively using the local phase information to enhance the various edges of ultrasound image. Specifically, we design the adaptive fractional order α based on PAS metric. We modify the adaptive fractional order strategy in [27] as follows

$$\alpha = 1 + \log_2\left(1 + PA^2\right) \quad (17)$$

where PA is the PAS metric.

The proposed adaptive strategy assigns low fractional order to preserve smooth regions and uses high fractional order to enhance edges. Furthermore, the PAS metric can show the edge significance of each point. As the PAS value increases, the edge significance of the point also increases. In other words, the point is more likely to be an edge point. According to (17), the fractional order α is a monotone increasing function of the PAS metric. A larger PAS metric yields a larger α which can produce better edge enhancement. Our method will adopt relatively high fractional order to enhance high significant edge points compared with the low significant edge points, so that we can properly preserve edges and obtain a better image enhancement.

B. Numerical Solver

We leverage the Euler-Lagrange equation [36] to solve the energy function (14). Assuming the solution u of this energy function $E(u)$ is known, then this solution must make $E(u)$ minimum. In other words, adding any slight perturbation to u will make the energy function larger. When the perturbation goes to 0, the derivative of the energy function with the respect to the perturbation is 0. The perturbation is represented as a very small continuous function $\eta \in C^{\infty}(\Omega)$ multiplied by a perturbation factor e. Define

$$\begin{aligned}&\Phi(e) := E(u + e\eta)\\ &= \int_{\Omega}\left[\varphi f\left(|\nabla^{\alpha}(u + e\eta)|\right) + \gamma\,|\nabla^{\alpha}(u + e\eta)|\right]dxdy\\ &+ \int_{\Omega}\left(\tfrac{\lambda}{2}\,|u + e\eta - u_0|^2\right)dxdy\end{aligned} \quad (18)$$

We first take the derivative of $\Phi(e)$ and obtain

$$\begin{aligned}&\Phi'(e) = \tfrac{d}{de}\Phi(e) =\\ &\varphi\int_{\Omega}\left(f'\left(|\nabla^{\alpha}(u + e\eta)|\right)\frac{\nabla_x^{\alpha}(u+e\eta)\,\nabla_x^{\alpha}\eta + \nabla_y^{\alpha}(u+e\eta)\,\nabla_y^{\alpha}\eta}{\sqrt{(\nabla_x^{\alpha}(u+e\eta))^2 + \left(\nabla_y^{\alpha}(u+e\eta)\right)^2}}\right)dxdy\\ &+\gamma\int_{\Omega}\left(\frac{\nabla_x^{\alpha}(u+e\eta)\,\nabla_x^{\alpha}\eta + \nabla_y^{\alpha}(u+e\eta)\,\nabla_y^{\alpha}\eta}{\sqrt{(\nabla_x^{\alpha}(u+e\eta))^2 + \left(\nabla_y^{\alpha}(u+e\eta)\right)^2}}\right)dxdy\\ &+\lambda\int_{\Omega}(u + e\eta - u_0)\eta dxdy,\end{aligned} \quad (19)$$

Let $e = 0$, we have

$$\begin{aligned}&\Phi'(0) =\\ &\varphi\int_{\Omega}\left(c\left(|\nabla^{\alpha} u|^2, PA^2\right)\left(\nabla_x^{\alpha} u\,\nabla_x^{\alpha}\eta + \nabla_y^{\alpha} u\,\nabla_y^{\alpha}\eta\right)\right)dxdy\\ &+\gamma\int_{\Omega}\frac{\nabla_x^{\alpha} u\,\nabla_x^{\alpha}\eta + \nabla_y^{\alpha} u\,\nabla_y^{\alpha}\eta}{|\nabla^{\alpha} u|}dxdy\\ &+\lambda\int_{\Omega}(u - u_0)\eta dxdy\end{aligned} \quad (20)$$

where $|\nabla^{\alpha} u| = \sqrt{\left(\nabla_x^{\alpha} u\right)^2 + \left(\nabla_y^{\alpha} u\right)^2}$. According to the previous analysis of how to find the solution u, we can obtain the conclusion that $\Phi'(0) = 0$. To simplify (20), we first use the definition of adjoint operator to simplify the following term

$$\nabla_x^{\alpha} u\,\nabla_x^{\alpha}\eta + \nabla_y^{\alpha} u\,\nabla_y^{\alpha}\eta = \left(\left(\nabla_x^{\alpha}\right)^*\nabla_x^{\alpha} u + \left(\nabla_y^{\alpha}\right)^*\nabla_y^{\alpha} u\right)\eta \quad (21)$$

where $\left(\nabla_x^{\alpha}\right)^*$ and $\left(\nabla_y^{\alpha}\right)^*$ are the adjoint operators of ∇_x^{α} and ∇_y^{α} respectively [37]. Based on the above analysis, we obtain the simplified form of (20) as follows

$$\begin{aligned}&\Phi'(0) =\\ &\varphi\int_{\Omega} c\left(|\nabla^{\alpha} u|^2, PA^2\right)\left(\left(\nabla_x^{\alpha}\right)^*\nabla_x^{\alpha} u + \left(\nabla_y^{\alpha}\right)^*\nabla_y^{\alpha} u\right)\eta\mathrm{d}x dy\\ &+\gamma\int_{\Omega}\frac{\left(\nabla_x^{\alpha}\right)^*\nabla_x^{\alpha} u + \left(\nabla_y^{\alpha}\right)^*\nabla_y^{\alpha} u}{|\nabla^{\alpha} u|}\eta\mathrm{d}x dy\\ &+\lambda\int_{\Omega}(u - u_0)\,\eta\mathrm{d}x dy\end{aligned} \quad (22)$$

Then, for all $\eta \in C^{\infty}(\Omega)$, we can obtain the Euler-Lagrange equation shown as

$$\begin{aligned}&\varphi c\left(|\nabla^{\alpha} u|^2, PA^2\right)\left(\left(\nabla_x^{\alpha}\right)^*\nabla_x^{\alpha} u + \left(\nabla_y^{\alpha}\right)^*\nabla_y^{\alpha} u\right)\\ &+\gamma\frac{\left(\nabla_x^{\alpha}\right)^*\nabla_x^{\alpha} u + \left(\nabla_y^{\alpha}\right)^*\nabla_y^{\alpha} u}{|\nabla^{\alpha} u|} + \lambda(u - u_0) = 0\end{aligned} \quad (23)$$

where u is the solution which makes the energy function minimum.

Let ∇E denotes the first derivative of the energy function $E(u)$, a necessary condition for u to be the extreme point of $E(u)$ is that $\nabla E = 0$ (Euler-Lagrange equation). So ∇E holds that

$$\begin{aligned}&\nabla E = \varphi c(|\nabla^{\alpha} u|^2, PA^2)((\nabla_x^{\alpha})^*\nabla_x^{\alpha} u + (\nabla_y^{\alpha})^*\nabla_y^{\alpha} u)\\ &+\gamma\frac{(\nabla_x^{\alpha})^*\nabla_x^{\alpha} u + (\nabla_y^{\alpha})^*\nabla_y^{\alpha} u}{|\nabla^{\alpha} u|} + \lambda(u - u_0)\end{aligned} \quad (24)$$

One way to find the desired u is using gradient descent method. Specifically, we introduce an artificial time parameter Δt and take small step in the direction of $-\nabla E$, *i.e.*, $u^{n+1} = u^n + \Delta t(-\nabla E)$. Finally, we will obtain the desired image u which makes the energy function $E(u)$ minimum.

C. Numerical algorithm

To compute (24) numerically, we use the G-L fractional differential to facilitate the numerical implementation. We assume that the size of a given image u is $X \times Y$, where X and Y are the numbers of pixels in vertical and horizontal direction

respectively. Then we can obtain the discretized schemes of $\nabla_{\mathrm{x}}^{\alpha}$, ∇_{y}^{α} , $(\nabla_{x}^{\alpha})^{*}$ and $\left(\nabla_{y}^{\alpha}\right)^{*}$ shown as follows

$$\begin{cases} \nabla_{x}^{\alpha} u_{i.j} = \sum_{l=0}^{j} (-1)^{l} \binom{\alpha}{l} u_{i,j-l} \\ \nabla_{y}^{\alpha} u_{i.j} = \sum_{l=0}^{i} (-1)^{l} \binom{\alpha}{l} u_{i-l,j} \end{cases} \tag{25}$$

$$\begin{cases} (\nabla_{x}^{\alpha})^{*} u_{i.j} = \sum_{l=0}^{Y-1-j} (-1)^{k} \binom{\alpha}{l} u_{i,j+l} \\ \left(\nabla_{y}^{\alpha}\right)^{*} u_{i.j} = \sum_{l=0}^{X-1-i} (-1)^{k} \binom{\alpha}{l} u_{i+l,j} \end{cases} \tag{26}$$

where $i = 0, 1, ..., X-1, j = 0, 1, ..., Y-1$, the formula $\binom{\alpha}{l}$ is the binomial coefficient defined as $\binom{\alpha}{l} = \frac{\Gamma(\alpha+1)}{\Gamma(l+1)\Gamma(\alpha-l+1)}$, here Γ is the gamma function. Let

$$\begin{cases} FAD_{\mathrm{x}} u_{i,j} = \sum_{l=0}^{Y-1-j} (-1)^{l} \binom{\alpha}{l} \frac{k_1^2 \nabla_x^{\alpha} u_{i,j+l}}{k_1^2 + |\nabla^{\alpha} u_{i,j+l}|^2 [1 + 254 PA(u_{i,j+l})]^2} \\ FAD_{y} u_{i,j} = \sum_{l=0}^{X-1-i} (-1)^{l} \binom{\alpha}{l} \frac{k_1^2 \nabla_y^{\alpha} u_{i+l,j}}{k_1^2 + |\nabla^{\alpha} u_{i+l,j}|^2 [1 + 254 PA(\mathrm{u}_{i+l,j})]^2} \end{cases} \tag{27}$$

$$\begin{cases} FTV_{x}\, u_{i,j} = \sum_{l=0}^{Y-1-j} (-1)^{l} \binom{\alpha}{l} \frac{\nabla_x^{\alpha} u_{i,j+l}}{\sqrt{(\nabla_x^{\alpha} u_{i,j+l})^2 + \left(\nabla_y^{\alpha} u_{i,j+l}\right)^2 + \varepsilon}} \\ FTV_{y}\, u_{i,j} = \sum_{l=0}^{X-1-i} (-1)^{l} \binom{\alpha}{l} \frac{\nabla_y^{\alpha} u_{i+l,j}}{\sqrt{(\nabla_x^{\alpha} u_{i+l,j})^2 + \left(\nabla_y^{\alpha} u_{i+l,j}\right)^2 + \varepsilon}} \end{cases} \tag{28}$$

where $PA(u_{i,j})$ is the PAS value of pixel $u_{i,j}$, ε is very small positive number. We summarize the optimization process in Algorithm 1.

Algorithm 1 Feature-preserving speckle reduction.

Input: noisy ultrasound image u_0, the values of s, k_0, time step Δt and iteration number n_{iter}

Output: the despeckled image u

1: Initialize $u^{(0)} = u_0, \varepsilon = 0.0001, n = 1$,
2: **for all** $n < n_{iter}$ **do**
3: Compute $FAD_x\, u_{i,j}^{(n)}, FAD_y\, u_{i,j}^{(n)}, FTV_x\, u_{i,j}^{(n)}$ and $FTV_y\, u_{i,j}^{(n)}$ using (27) and (28)
4: Compute $u^{(n+1)}$ through the following procedure: $u_{i,j}^{(n+1)} = u_{i,j}^{(n)} - \Delta t[\varphi(FAD_x\, u_{i,j}^{(n)} + FAD_y\, u_{i,j}^{(n)}) + \gamma(FTV_x\, u_{i,j}^{(n)} + FTV_y\, u_{i,j}^{(n)}) + \lambda(u_{i,j}^{(n)} - u_{i,j}^{(0)})]$
5: Set $n = n + 1$
6: **end for**
7: Set the despeckled image $u = u^{(n)}$
8: **return** u

IV. EXPERIMENTAL RESULTS

In this section, experiments with synthetic and clinic ultrasound images were carried out to show the performance of our method[1]. Several well-known ultrasound despeckling filters were used for comparison, including Frost [9], SRAD [15], OBNLM [11], SBF [10], ADLG [2], NLLRF [12]. We directly asked the source code of SBF filter from its authors. As for other filters, we can obtain the source codes from the cited authors' websites listed in their works.

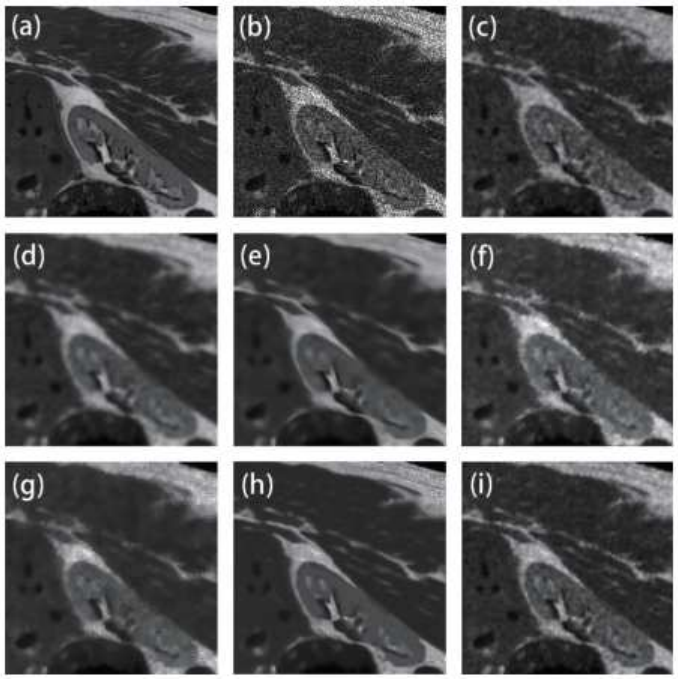

Fig. 3. Results of different filters for the synthetic image. (a) Original image, (b) original image corrupted with speckle noise with variance $\sigma^2 = 0.2$, despeckled result by (c) Frost ($W = 5 \times 5$) , (d) SRAD ($\Delta t = 0.3, n_{iter} = 60$), (e) OBNLM ($M = 5, \alpha = 6, h = 3$) , (f) SBF ($W$=$3 \times 3, \mathrm{n_{iter}} = 9$), (g) ADLG ($\Delta \mathrm{t} = 0.3, n_{iter} = 50$), (h) NLLRF ($\beta = 20, H = 10$), (i) our method ($\Delta t = 0.3, s = 20, k_0 = 100, n_{iter} = 7$).

A. Synthetic image experiment

For the purpose of quantitative comparisons, we generated noise over the ground truth image by employing the synthetic speckle noise model which is widely used in literature [11], [12], [21]. The noise model is given by

$$u(x_i) = v(x_i) + v(x_i)\tau(x_i), \tau(x_i) \sim N(0, \sigma^2) \tag{29}$$

where $v(x_i)$ and $u(x_i)$ are the pixel intensities of pixel x_i in the noise-free image and the synthesized noisy image respectively, and $\tau(x_i)$ is a zero-mean Gaussian noise with variance σ^2. We applied this noise model to the Fig. 3(a) which consists of smooth regions and various local features. There levels of noise were tested by setting $\sigma^2 = \{0.2; 0.4; 0.6\}$. Fig. 3(b) depicts the synthetic image with noise variance σ^2 =0.2.

To quantitatively evaluate the performance of each filter, peak signal-to-noise ratio (PSNR), mean structural similarity (MSSIM) [38] and feature similarity index (FSIM) [39] were adopted in this paper. Specifically, FSIM (the Matlab code is available at[2]) is designed for measuring the ability of preserving features, and it takes values between 0 and 1, and 1 denotes the best performance of feature preservation.

[1]The source code for the reproducible research will be available after paper acceptance at http://www.escience.cn/people/bjqin/research.html

[2]http://sse.tongji.edu.cn/linzhang/IQA/FSIM/FSIM.htm

TABLE I
COMPARISON OF THE PSNR, MSSIM AND FSIM VALUES AMONG DIFFERENT FILTERS.

	PSNR			MSSIM			FSIM		
	0.2	0.4	0.6	0.2	0.4	0.6	0.2	0.4	0.6
Frost	25.773	23.840	22.955	0.721	0.638	0.576	0.848	0.818	0.797
SRAD	26.760	25.272	24.282	0.743	0.697	0.679	0.816	0.777	0.764
OBNLM	26.496	24.974	24.121	0.742	0.696	0.679	0.822	0.794	0.764
SBF	22.502	22.303	22.214	0.695	0.648	0.657	0.825	0.807	0.790
ADLG	24.585	22.945	22.360	0.676	0.625	0.599	0.786	0.758	0.745
NLLRF	27.409	25.536	24.282	0.763	0.711	0.699	0.825	0.798	0.768
Ours	**27.721**	**25.994**	**25.103**	**0.783**	**0.732**	**0.713**	**0.867**	**0.844**	**0.834**

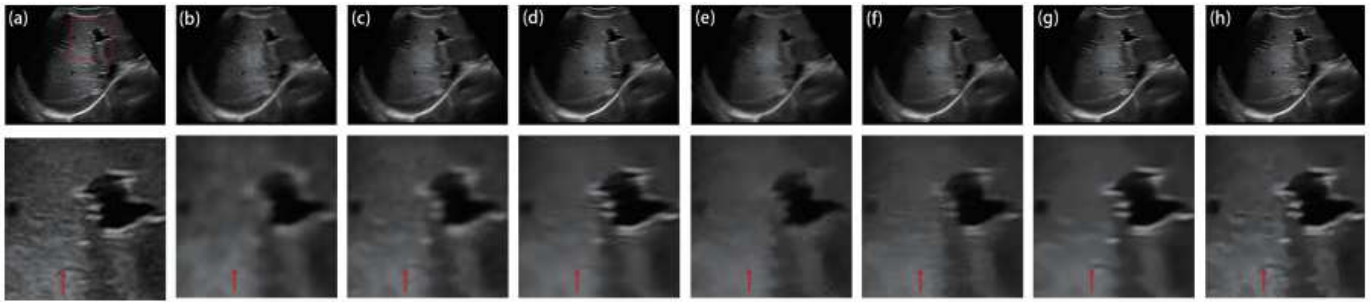

Fig. 4. Despeckled results of the ultrasound image of liver trauma and the corresponding zoomed details. (a) The original image; results by (b) Frost, (c) SRAD, (d) OBNLM, (e) SBF, (f) ADLG, (g) NLLRF, (h) our method.

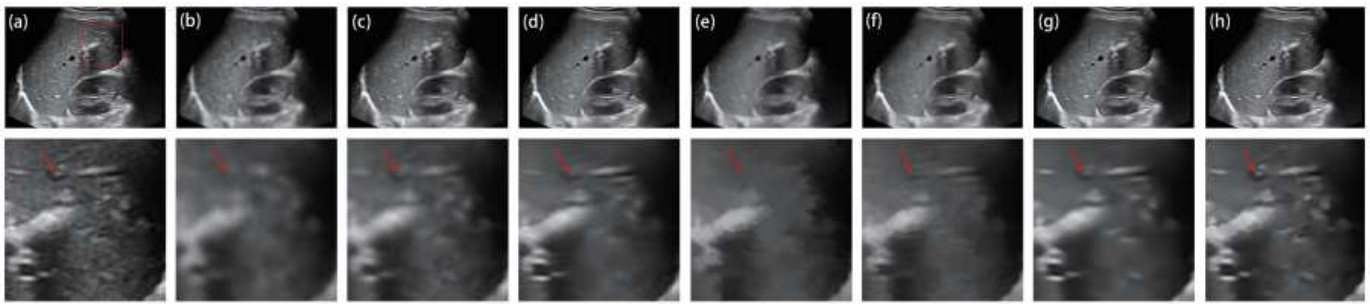

Fig. 5. Despeckled results of the ultrasound image of hepatitis and the corresponding zoomed details. (a) The original image; results by (b) Frost, (c) SRAD, (d) OBNLM, (e) SBF, (f) ADLG, (g) NLLRF, (h) our method.

To compare the performance of each filter fairly, each filter needs to achieve the best performance by setting its optimal parameters. The optimal parameters need to be selected based on a quantitative metric so that the PSNR metric is accepted as a gold standard as in [40]. Therefore, we obtain its optimal parameters of each filter when achieving the highest value of the PSNR metric. Specifically, our method contains the following parameters: s is the scale of Cauchy kernel, Δt is the time step, n_{iter} is the iteration number, and k_0 is a parameter related with noise level.

Fig. 3 depicts the denoised images of different filters with their optimal parameters. Frost filter has clear features, but it retains a significant level of noise. SRAD remove noise better but produces smoother edges and removes some low contrast features compared with Frost. Though OBNLM and NLLRF have good performance in high contrast features, they cause some meaningful low contrast features becoming indiscernible after noise removal. Both SBF and ADLG produce fuzzy boundaries, and ADLG removes lots of details. Our method achieves best performances in noise removal and feature preservation.

Table I compares the PSNR, MSSIM and FSIM values for different filters. Our method achieves the highest PNSR, MSSIM and FSIM. The highest PSNR denotes that the despeckled image of our method produces the lower image distortion compared with other filters. The highest MSSIM represents that the despeckled image of our method is the most similar to the original image. The highest FSIM represents that our method outperforms other filters in feature preservation.

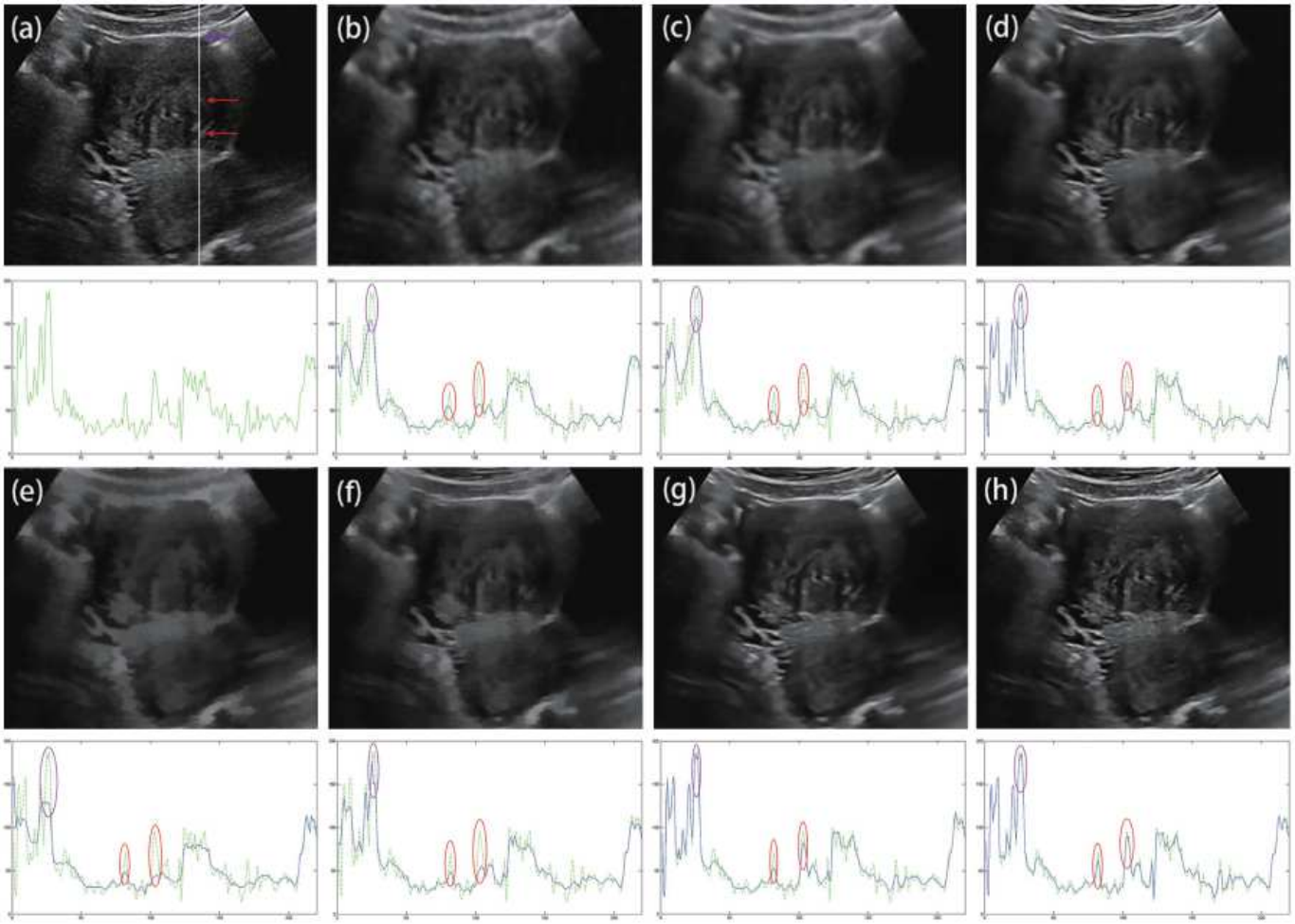

Fig. 6. Despeckled results of the ultrasound image of uterine fibroids and the corresponding scan column. The green line is the processed result of original image while the blue line is the processed result of each filter. (a) The original image; results by (b) Frost, (c) SRAD, (d) OBNLM, (e) SBF, (f) ADLG, (g) NLLRF, (h) our method.

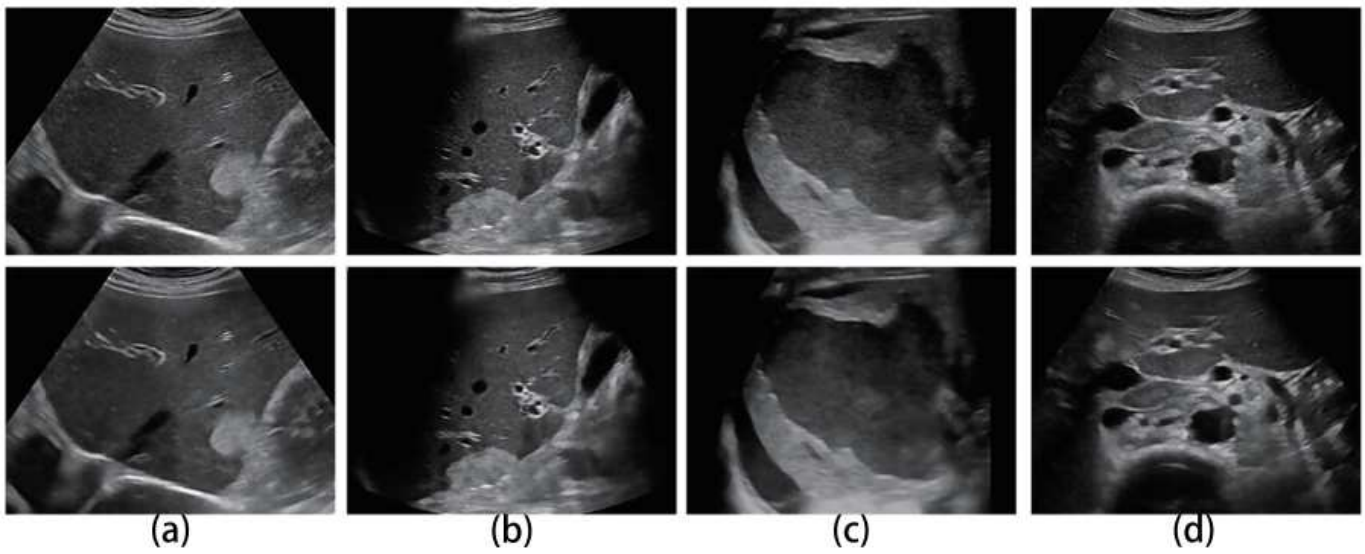

Fig. 7. More despeckled results of our method. First row: original ultrasound images; second row: the despeckled results. (a) ultrasound image of hemangiomas, ultrasound (b) image of hemangiomas, (c) ultrasound image of spleen trauma, (d) ultrasound image of retroperitoneal lymphe nodes and tumors image.

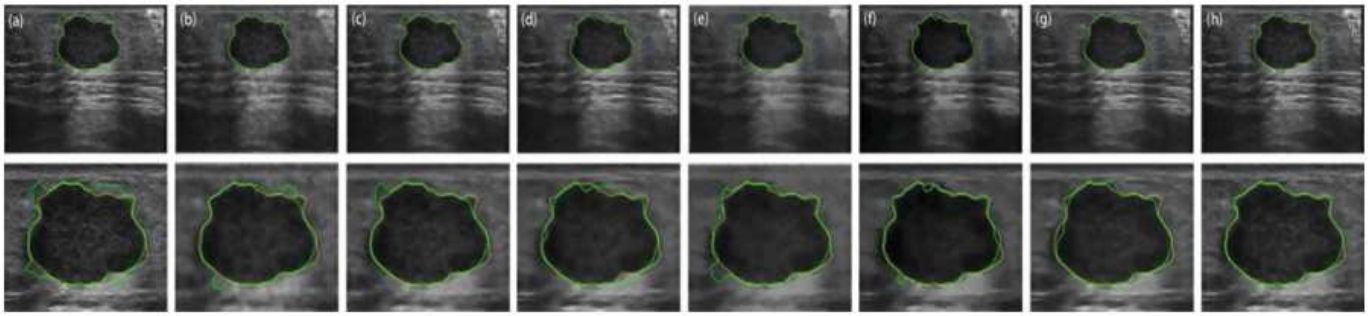

Fig. 8. The comparison of breast tumor segmentation on different despeckled results. Yellow color: the ground truth delineated by an experienced clinician; Green color: the segmentation results produced by [42]. (a) The original ultrasound image and its segmentation result. Despeckled result and the corresponding segmentation results by (b) Frost, (c) SRAD, (d) OBNLM, (e) SBF, (f) ADLG, (g) NLLRF, (h) our method.

B. Clinic image experiment

Since real ultrasound images are all affected by speckle noise, there is no ground truth image. Therefore, we cannot calculate the values of the PSNR, MSSIM and FSIM. We employed different types of clinic ultrasound images to visually verify the performance of our method. The clinic ultrasound images were all downloaded from the website.[3]

Different from the synthetic image experiment, real image experiment has no gold standard to find the optimal parameters. We adjust the parameters for each filter to obtain the best visual effect. The final optimal parameter configurations for all filters are set as: 1) Frost: $W = 5 \times 5$, 2) SRAD: $\Delta t = 0.1, n_{iter} = 120$, 3) OBNLM: $M = 3, \alpha = 6, h = 1$, 4) SBF: $W{=}3 \times 3, \mathrm{n_{iter}} = 15$, 5) ADLG: $\Delta \mathrm{t} = 0.15, n_{iter} = 80$, 6) NLLRF: $\beta = 10, H = 10$, 7) our method: $\Delta t = 0.15, s = 15, k_0 = 20, n_{iter} = 8$. Then, the filters were applied to clinic ultrasound images with their own parameter configurations.

Fig. 4 and Fig. 5 depict the despeckled results of different filters in the first row and show the corresponding local zoomed-in results in the second row. Visually, our method achieves the best performances in feature preservation and noise removal. According to the streak shown by the red arrow in Fig. 4, our method produces the clearest edges. NLLRF only preserves a part of the streak while SRAD reduce the contrast of the streak heavily. Other filters remove the streak after speckle reduction. Similarly, according to the nodules indicated by the red arrow in Fig. 5, our method succeeds in enhancing the local contrast. SRAD, OBNLM and NLLRF reduce the contrast of the nodules heavily. Other filters remove the nodules after despeckling.

To more closely evaluate despeckled images of different filters, we adopted the method in [41] which evaluates all the features located in a single scan line through the ultrasound image. Fig. 6 shows the desepckled images of different filters and their corresponding scan column. The scan line shows that, Frost, SRAD, SBF and ADLG all fail to keep the edge contrast, reducing the visual effect. OBNLM and NLLRF succeed in enhancing high contrast edges shown by the purple window. As for low contrast edges, OBNLM and NLLRF both fail to preserve the local contrast indicated by the red windows. As shown by the red windows in Fig. 6(h), after edge enhancement using adaptive fractional-order α, there are slight differences of edge contrast between the despeckled image of our method and the original ultrasound image. Compared with other filters, our method achieves the best performance in preserving the edge contrast. More despeckled results are depicted in Fig. 7. Obviously, our method removes speckle noise thoroughly while preserving features satisfactorily.

[3]http://www.ultrasoundcases.info

TABLE II
MEAN DSC, JS, HD AND HM VALUES FOR DIFFERENT SEGMENTATION RESULTS ON TEN BREAST ULTRASOUND IMAGES.

	DSC(%)	JS(%)	HD	HM
Input	91.87	85.02	16.9933	3.3599
Frost	93.62	88.02	9.8418	2.1265
SRAD	94.02	90.52	8.2271	1.5781
OBNLM	95.64	90.89	8.0608	1.6167
SBF	93.65	87.66	12.8664	2.0820
ADLG	94.92	90.37	9.0798	1.7034
NLLRF	95.39	91.21	7.2801	1.4977
our method	**96.25**	**92.06**	**4.8441**	**1.2108**

TABLE III
MEDIAN DSC, JS, HD AND HM VALUES FOR DIFFERENT SEGMENTATION RESULTS ON TEN BREAST ULTRASOUND IMAGES.

	DSC(%)	JS(%)	HD	HM
Input	91.63	84.56	16.8859	3.1183
Frost	93.12	87.12	8.9443	1.9195
SRAD	95.27	90.97	8.0868	1.5573
OBNLM	95.45	91.03	6.6623	1.6149
SBF	94.19	89.02	13.3033	1.9863
ADLG	94.99	90.49	8.0007	1.6920
NLLRF	95.5	91.39	7.0000	1.4623
our method	**96.15**	**92.59**	**4.6926**	**1.3004**

C. Application to ultrasound image segmentation

For further validating the performance of our method, we apply each filter to breast ultrasound (BUS) image segmentation. BUS images are commonly used to differentiate between

benign and malignant tumors, which can be characterized by their shapes or contours of segmented breast lesions [2]. We first despeckle ten breast ultrasound images with different lesions by using different filters. Then, we employ a famous level-set method [42] to segment the despeckled results. Fig. 8 shows an example of a BUS image, the green curves are the segmentation results of different filters and the yellow curve is delineated by an experienced clinician, which is usually regarded as the ground truth. As depicted in Fig. 8, after the speckle reduction, each filter improves the performance of the segmentation result compared with the original BUS image. Among these filters, the segmentation result of the proposed filter is closest to the ground truth. The enhanced lesions are blurry in other despeckled images by other filters so that the segmentation method [42] is not able to accurately segment the lesion contours from the different despeckled images.

We further adopt four metrics containing dice similarity coefficient (DSC) [22], Jaccard similarity (JS) [43], Hausdorff distance (HD) [44] and Hausdorff mean (HM) [44] to measure the segmentation accuracy. DSC and JS measure the overlapping rate between the obtained segmentation region and the ground truth, while HD and HM compute the distance of the contours between the obtained segmentation region and the ground truth. Hence, a better segmentation result should have higher DSC and JS, as well as lower HD and HM. Table II and Table III list the mean and median values of DSC, JS, HD and HM for different segmentation results on ten despekcled BUS images, respectively. Obviously, the proposed method achieves the largest DSC and JS values, as well as the smallest HD and HM values. These results indicate that the proposed method achieves better segmentation performance compared with other filters.

V. Discussion and Conclusion

Due to the outstanding performance, non-local filtering is becoming a widely accepted method in image restoration and denoising [45]. In ultrasound despeckling, several state-of-the-art non-local filters [1], [3], [4], [11], [12], [46] were developed recently. Compared with other despeckling techniques, they all achieved the best performance of preserving features. To verify the performance of our method, two non-local filters including OBNLM and NLLRF were used for comparison. We find that non-local filters make some low contrast features heavily blurred. This is due to the fact that the patches around these features are pretty similar to the patch centered at speckle noise. After non-local filters remove noise by a weighted average of similar features, these low contrast features will become indiscernible [21]. Compared with non-local filters, our method performs better in preserving features while removing noise thoroughly.

In conclusion, we have proposed a phase asymmetry guided adaptive total variation and diffusion filter for feature-preserving ultrasound despeckling. According to the PAS metric in accurately representing edge features, we properly combine FAD filter and FTV filter to achieve the best performance of preserving the edge features in the transition border regions between the homogeneous regions of different tissues. Moreover, we also integrate the PAS metric into the diffusion coefficient to preserve low contrast edges. We further design the adaptive fractional-order α to enhance various edges with different significances in ultrasound images. Experiments with synthetic and clinic ultrasound images indicate that our method outperforms other well-known ultrasound despeckling filters in both speckle reduction and feature preservation.

Acknowledgment

This work was supported by NSFC Grants 61271320 and Medical Engineering Cross Fund of Shanghai Jiao Tong University (YG2014MS29). BF was partially supported by NIH Grants R01CA156775, R21CA176684, and R01CA204254, and R01HL14024. The authors would like to thank all the cited authors for providing the source codes used in this work and the anonymous reviewers for their valuable comments on this paper.

References

[1] Zhan Y, Ding M, Wu L, et al. Nonlocal means method using weight refining for despeckling of ultrasound images, Signal Processing, 2014, 103(C):201-213.
[2] Flores WG, and et al. Breast Ultrasound Despeckling Using Anisotropic Diffusion Guided by Texture Descriptors, Ultrasound in Medicine & Biology, 2014, 40(11):2609-21.
[3] Song P, Trzasko JD, Manduca A, Huang R, Kadirvel R, Kallmes DF, and Chen S, Improved Super-Resolution Ultrasound Microvessel Imaging With Spatiotemporal Nonlocal Means Filtering and Bipartite Graph-Based Microbubble Tracking. IEEE transactions on ultrasonics, ferroelectrics, and frequency control, 2018, 65(2):149-167.
[4] Afsham N, Rasoulian A, Najafi M, Abolmaesumi P, and Rohling R, Nonlocal means filter-based speckle tracking. IEEE transactions on ultrasonics, ferroelectrics, and frequency control, 2015, 62(8):1501-1515.
[5] Wagner RF, Smith SW, Sandrik JM, et al. Statistics of Speckle in Ultrasound B-Scans, IEEE Trans. Son. Ultrason, 2005, 30(3):156-163.
[6] Osman FM, Yap MH, The effect of filtering algorithms for breast ultrasound lesions segmentation. Informatics in Medicine Unlocked. 2018, 12:14-20.
[7] Choi H, Jeong, J, Despeckling images using a preprocessing filter and discrete wavelet transform-based noise reduction techniques. IEEE Sensors Journal, 2018, 18(8):3131-3139.
[8] Bao L, Song Y, Yang Q, et al. Tree Filtering: Efficient Structure-Preserving Smoothing With a Minimum Spanning Tree, IEEE Trans. Image Proc., 2014, 23(2):555-69.
[9] Frost VS, Stiles JA, Shanmugan KS, et al. A model for radar images and its application to adaptive digital filtering of multiplicative noise, IEEE Trans. Pattern Anal. Mach. Intell., 1982, 4(2):157-66.
[10] Tay PC, Garson CD, Acton ST, et al. Ultrasound despeckling for contrast enhancement, IEEE Trans. Image Proc., 2010, 19(7):1847-60.
[11] Coupe P, Hellier P, Kervrann C, et al. Nonlocal means-based speckle filtering for ultrasound images, IEEE Trans. Image Proc., 2009, 18(10):2221-9.
[12] Zhu L, Fu CW, Brown MS, et al. A Non-local Low-Rank Framework for Ultrasound Speckle Reduction, IEEE Conference on Computer Vision and Pattern Recognition, 2017:493-501.
[13] Zhao W, Lv Y, Liu Q, Qin B, Detail-preserving image denoising via adaptive clustering and progressive PCA thresholding, IEEE Access, 2018, 6:6303-15.
[14] Perona P and Malik J, Scale-space and edge detection using anisotropic diffusion, IEEE Trans. Pattern Anal. Mach. Intell., 1990, 12(7):62939.
[15] Yu Y, Acton ST. Speckle reducing anisotropic diffusion, IEEE Trans. Image Proc., 2002, 11(11):1260-70.
[16] Aja-Fernndez S, Alberola-Lpez C. On the estimation of the coefficient of variation for anisotropic diffusion speckle filtering, IEEE Trans. Image Proc., 2006, 15(9):2694.
[17] Krissian K, Westin CF, Kikinis R, et al. Oriented Speckle Reducing Anisotropic Diffusion, IEEE Trans. Image Proc., 2007, 16(5):1412-24.
[18] Bai J, Feng XC. Fractional-Order Anisotropic Diffusion for Image Denoising, IEEE Trans. Image Proc., 2007, 16(10):2492-502.

[19] Qiu Z, Yang L, Lu W. A New Feature-preserving Nonlinear Anisotropic Diffusion Method for Image Denoising, BMVC. 2011.
[20] Khodadadi H, Aghdam A G, Rivaz H. Edge-preserving ultrasonic strain imaging with uniform precision. Conf Proc IEEE Eng Med Biol Soc, 2015, 2015:3835-38.
[21] Zhu L, Wang W, Qin J, et al. Fast feature-preserving speckle reduction for ultrasound images via phase congruency, Signal Processing, 2017, 134:275-84.
[22] Belaid A, Boukerroui D, Maingourd Y, et al. Phase-based level set segmentation of ultrasound images, IEEE Trans. Infor. Tech. Biomed., 2011, 15(1):138-47.
[23] Kovesi P. Symmetry and Asymmetry from Local Phase, Tenth Australian Joint Converence on Artificial Intelligence, 1997:2-4.
[24] Zhou G Q, Jiang W W, Lai K L, et al. Automatic Measurement of Spine Curvature on 3-D Ultrasound Volume Projection Image With Phase Features, IEEE Trans. Med. Imaging, 2017, 36(6):1250-62.
[25] Zhao Y, Zhao Y, Zheng Y, et al. Automatic 2D/3D Vessel Enhancement in Multiple Modality Images Using a Weighted Symmetry Filter, IEEE Trans. Med. Imaging, 2018, 37(2):438-50.
[26] Kovesi P. Image Features From Phase Congruency, Journal of Computer Vision Research, 1999, 1(1):115-16.
[27] Zhou Q, Gao J, Wang Z, et al. Adaptive Variable Time Fractional Anisotropic Diffusion Filtering for Seismic Data Noise Attenuation, IEEE Trans. Geoscience & Remote Sensing, 2016, 54(4):1905-17.
[28] Yu J, Tan L, Zhou S, et al. Image Denoising Algorithm Based on Entropy and Adaptive Fractional Order Calculus Operator, IEEE Access, 2017, 5:12275-12285.
[29] Felsberg M, Sommer G. The monogenic signal, IEEE Press, 2001.
[30] Boukerroui D, Noble JA, Brady M. On the Choice of Band-Pass Quadrature Filters, J. Math. Imaging Vis., 2004, 21(1-2):53-80.
[31] Love ER. Fractional Derivatives of Imaginary Order, Journal of the London Mathematical Society, 1971, s2-3(2):241-59.
[32] Oldham KB, Spanier. (1974) The fractional calculus: integrations and differentiations of arbitrary order, Academic Press, New York.
[33] Yi F, WANG WX, et al. Fractional differential approach to detecting textural features of digital image and its fractional differential filter implementation, Science in China, 2008, 51(9):1319-39.
[34] Ruding L, Osher S, and FatemiI E. Nonlinear Total Variation Based Noise Removal Algorithms. Phys. D, 1992, 60(1-4):259-68.
[35] Zhang J, Wei Z. Fractional Variational Model and Algorithm for Image Denoising, IEEE International Conference on Natural Computation, 2008:524-528.
[36] Riley KF, Hobson MP, Bence SJ, Mathematical Methods for Physics and Engineering: A Comprehensive Guide, 3rd Edition, Cambridge University Press, 2006.
[37] Wang D, Gao J. A new method for random noise attenuation in seismic data based on anisotropic fractional-gradient operators, Journal of Applied Geophysics, 2014, 110:135-143.
[38] Wang Z, Bovik AC, Sheikh HR, et al. Image quality assessment: from error visibility to structural similarity, IEEE Trans. Image Proc., 2004, 13(4):600.
[39] Zhang L, Zhang L, Mou X, et al. FSIM: A Feature Similarity Index for Image Quality Assessment, IEEE Trans. Image Proc., 2011, 20(8):2378-2386.
[40] Ramosllordn G, Vegassnchezferrero G, Martinfernandez M, et al. Anisotropic diffusion filter with memory based on speckle statistics for ultrasound images, IEEE Trans. Image Proc. 2015, 24(1):345-358.
[41] Aysal TC, Barner KE. Rayleigh-maximum-likelihood filtering for speckle reduction of ultrasound images, IEEE Trans. Med. Imaging, 2007, 26(5):712.
[42] C. Li, C. Xu, C. Gui, M.D. Fox, Distance regularized level set evolution and its application to image segmentation. IEEE Trans. Image Process, 2010, 19(12):32433254.
[43] Udupa J K, Imielinska C, Saha P K, et al. Methodology for evaluating image-segmentation algorithms[J]. Proceedings of SPIE - The International Society for Optical Engineering, 2002, 4684(4684):266-277.
[44] Cardoso F M, Matsumoto M M S, Furuie S S. Edge-Preserving Speckle Texture Removal by Interference-Based Speckle Filtering Followed by Anisotropic Diffusion[J]. Ultrasound in Medicine & Biology, 2012, 38(8):1414-1428.
[45] Shao L, Yan R, Li X, et al. From heuristic optimization to dictionary learning: a review and comprehensive comparison of image denoising algorithms, IEEE Trans. Cyber., 2014, 44(7):1001-1013.
[46] Santos CAN, Martins DLN, Mascarenhas N D A. Ultrasound Image Despeckling Using Stochastic Distance-Based BM3D, IEEE Trans. Image Proc., 2017, 26(6):2632-2643.